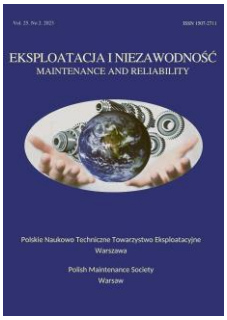

Eksploatacja i Niezawodnosc – Maintenance and Reliability

Volume 28 (2026), Issue 4

journal homepage: http://www.ein.org.pl

Article citation info:
Yi H, Fan Z, Qin W, Zhang H, Zhao J, Adaptive force control for time-varying parameter systems in film peeling, Eksploatacja i Niezawodnosc – Maintenance and Reliability 2026: 28(4) http://doi.org/10.17531/ein/220212

Adaptive force control for time-varying parameter systems in film peeling

Indexed by: Web of Science Group

Haoran Yi[a], Zhibin Fan[a], Wenlei Qin[a], He Zhang[a,*], Jie Zhao[a]

[a] Harbin Institute of Technology, China

Highlights

- Novel adaptive force controller designed for systems with time-varying parameters.
- Proposed controller eliminates abrupt output changes from sliding mode control.
- Experimental validation confirms enhanced robotic film peeling safety.

Abstract

This paper proposes an adaptive force-tracking controller for nonlinear systems with time-varying parameters, based on the practical task of peeling a film from the surface of a rigid body. The precise regulation of the peeling force by a force controller during robotic film peeling is critical for enhancing the safety and stability of the operation. Existing adaptive controllers for systems with time-varying parameters either result in large tracking errors or can only achieve closed-loop system stability, failing to track the desired force. The proposed controller employs the congelation of variables and robust adaptive control. The stability of the closed-loop system demonstrated via the corresponding Lyapunov function. Subsequent simulation results show that the tracking error of the closed-loop system with the proposed controller asymptotically converges to zero, validating the theoretical approach. Finally, experiments not only confirm the feasibility and stability of the proposed controller but also successfully demonstrate its potential for application in robotics.

Keywords
adaptive control, nonlinear systems, time-varying parameters

1. Introduction

Peeling an adhesive film from a rigid surface is a common and necessary operation in daily life, industrial, and medical fields. Using robots to perform film peeling aligns with the current trend of automation and intelligence across various sectors. In applications such as using robots to peel protective films from painted metal surfaces, excessive peeling force can cause the film to break or even damage the paint, significantly reducing production efficiency and operational reliability. Similarly, in retinal microsurgery for membrane peeling, excessive force may lead to retinal hemorrhageb [1]. Therefore, stable control of the peeling force plays an indispensable role in robotic film detachment operations. According to Peng and Yin's paper [2–4], the force required to peel a film from a rigid surface depends on the film's width, thickness, peeling angle, and material properties. Except for the material properties, all other factors can be time-varying in practice. Therefore, force control for film peeling essentially involves force control for a system with time-varying parameters.

Adaptive control is a technique designed for nonlinear dynamic systems with unknown parameters, capable of simultaneously ensuring closed-loop stability in both tracking error and parameter estimation error. Although significant progress has been made in adaptive controllers since the 1980s [5–9], research on adaptive controllers for time-varying

(*) Corresponding author.
E-mail addresses: H. Yi (ORCID: 0000-0001-5803-106X) 21b908038@stu.hit.edu.cn, Z. Fan (ORCID: 0009-0009-8859-0677) zbfan@stu.hit.edu.cn, W. Qin,18B908096@hit.edu.cn, H. Zhang, zhanghe0451@hit.edu.cn, J. Zhao (ORCID: 0000-0002-6086-9387) jzhao@hit.edu.cn

unknown parameters remains limited compared to studies on traditional adaptive controllers [10,11]. The primary reason is that stability analysis in such cases introduces the derivative term of the parameters into the Lyapunov function.

Early research on adaptive controllers for systems with time-varying parameters found that by requiring bounded and slow parameter variations, stable tracking error results could be achieved [12,13]. Subsequent work began addressing the problem using robust adaptive control methods, such as σ -modification (σ -mod) [14] and adaptive sliding mode control [15]. The σ -mod introduces a leakage mechanism into the parameter update law, ensuring that parameter estimates remain within a predefined range. However, this method is only applicable to systems with slowly varying parameters and requires prior knowledge of the correct variation range of the parameters. Adaptive sliding mode control uses high-gain or high-frequency control outputs to counteract the effects of parameter variations. Yet, the absence of a feedforward term, along with excessively large or high-frequency control outputs, are inherent and unavoidable issues of this method.

More recent studies have discovered adaptive control methods for systems with rapidly varying parameters. For linear systems with vanishing time-varying parameters, the research by R. Marino demonstrates results with asymptotic convergence [16,17]. For nonlinear systems with periodic time-varying parameters of known period, the study by Xu also provides asymptotically convergent results [18]. However, these approaches all impose certain restrictions on the time-varying parameters and cannot be applied to systems with more general types of parameter variations. Furthermore, when the parameters vary persistently, none of the above methods can guarantee that the tracking error will asymptotically converge to zero.

In Zhang's research [19,20], he pointed out that the error in adaptive control originates from unknown parameter variations. Time-varying parameters are modeled as known parameter variations, while the discrepancy between the parameter model and the actual parameters constitutes the unknown parameter variations. Building on this theory, K. Chen recently proposed an adaptive controller design method called the congelation of variables [21]. This approach treats the unknown time-varying parameter as a combination of an unknown constant parameter and a time-varying disturbance. In other words, the time-varying parameters are " congealed " Subsequently, classical adaptive controllers are employed to handle the unknown constant part, while robust controllers are used to address the disturbance part. Consequently, the controller effectively integrates a traditional gradient update law-based adaptive controller with a high-gain robust controller. Although this approach can significantly reduce the gain of the robust controller and enable fast convergence in systems with time-varying parameters, it cannot be applied to asymptotic tracking problems.

Inspired by the congelation of variables, this paper proposes an adaptive force controller suitable for time-varying parameters. This controller integrates sliding mode control and adaptive control, but utilizes an integral action to eliminate the chattering issue inherent in sliding mode control, resulting in smoother control outputs. This makes the controller directly applicable to robots.

2. Adaptive control design and stability analysis

2.1. Dynamic model

The process of peeling a film from a rigid surface is illustrated in Figure 1. Based on the research by Peng, the dynamics of film peeling can be described by the following equation:

$$\frac{f}{w} = c(1 + mv^{0.4}) \tag{1}$$

where f is the peeling force. w is the film width. v is the peeling velocity. c and m are parameters related to the peeling angle φ and the film thickness h, respectively. Furthermore, the values of all the aforementioned parameters are always greater than zero.

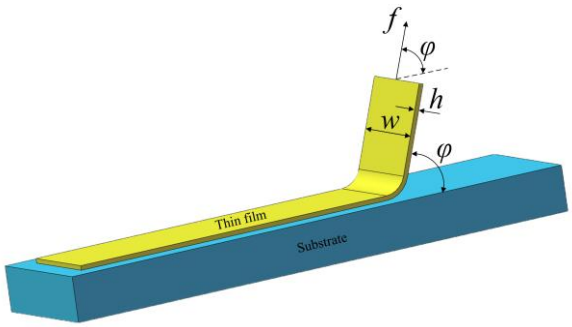

Figure 1. Schematic diagram of film peeling, illustrating the dimensions associated with the dynamic equations.

In the most extreme scenario, the width and thickness of the film being peeled, as well as the peeling angle, could all be time-

varying. However, to address more general conditions, this paper considers the thickness of the film as constant, meaning parameter is treated as an unknown constant.

By rearranging Equation (1), we obtain:

$$\frac{f}{w \cdot c \cdot m} = v^{0.4} + \frac{1}{m} \tag{2}$$

Given that c and w are time-varying variables and all parameters are greater than zero, the following expression can be derived:

$$a(t) \cdot f = v^{0.4} + m_0 \tag{3}$$

where $a(t) = \frac{1}{w \cdot c \cdot m}$, $m_0 = \frac{1}{m}$. Empirical and experimental data indicate that when $v \geq 0, f \geq 0$, and both are bounded. Therefore, $a(t)$ and m_0 are bounded and strictly positive.

2.2. Adaptive Controller Design

Since most robots are controlled by position or velocity loops and cannot directly control acceleration, the velocity $v^{0.4}$ is selected as the control input, i.e., $u = v^{0.4}$. Differentiating Equation (3) yields:

$$\dot{a} \cdot f + a \cdot \dot{f} = \dot{u} \tag{4}$$

Further manipulation yields:

$$\dot{f} = \frac{-\dot{a}}{a} \cdot f + \frac{1}{a} \cdot \dot{u} \tag{5}$$

By introducing additional simplifications to the parameters, we obtain:

$$\dot{f} = \theta(t) \cdot f + b(t) \cdot \dot{u} \tag{6}$$

where $\theta(t) = \frac{-\dot{a}}{a}$, $b(t) = \frac{1}{a}$. Since $a(t)$ and $\dot{a}(t)$ are bounded and strictly positive, $\theta(t)$ must be bounded, and $b(t)$ is also bounded and strictly positive.

Following the philosophy of the congelation of variables, Equation (6) can be rewritten as:

$$\dot{f} = \hat{\theta} f + \Delta_\theta f + (\ell_\theta - \hat{\theta}) f + \bar{\dot{u}} + \Delta_b \hat{\rho} \bar{\dot{u}} - \ell_b (\frac{1}{\ell_b} - \hat{\rho}) \bar{\dot{u}} \tag{7}$$

where $\dot{u} = \hat{\rho} \bar{\dot{u}}$, $\Delta_\theta = \theta(t) - \ell_\theta$, $\Delta_b = b(t) - \ell_b$. $\hat{\theta}$ and $\hat{\rho}$ are the estimates of ℓ_θ and $\frac{1}{\ell_b}$, respectively. ℓ_θ and ℓ_b are constants parameters, while Δ_θ and Δ_b are time-varying disturbances. The value of ℓ_θ is typically selected to minimize $|\Delta_\theta|$, while ℓ_b must satisfy $0 < \ell_b < b(t)$ for all $t \geq 0$.

Based on the above conclusions, we propose the following adaptive force controller for systems with time-varying parameters:

$$\bar{\dot{u}} = -ke - \delta_\theta |f| sgn(e) - |\dot{f}_d| sgn(e) - \frac{1}{2}\left(\varepsilon_\theta + \frac{\hat{\theta}^2 f^2}{\varepsilon_\theta}\right) sgn(e) \tag{8}$$

$$\dot{\hat{\theta}} = \alpha f e \tag{9}$$

$$\dot{\hat{\rho}} = -\gamma \bar{\dot{u}} e \cdot sgn(\ell_b) = -\gamma \bar{\dot{u}} e \tag{10}$$

where k, α and γ are all greater than zero, representing the force gain and adaptive gains, respectively. f_d is the desired force, which can be either a constant or a variable. $e = f - f_d$, $\delta_\theta = max(|\Delta_\theta|)$.The function $sgn(e)$ is signum function of the error e (where $sgn(e) = 0$ when $e = 0$), and similarly for $sgn(\ell_b)$. $\varepsilon_\theta > 0$is a constant used to balance the linear and nonlinear terms.

During the analysis of the dynamic equation (Equation (7)), we employed the congelation of variables. The time-varying parameter $\theta(t)$ is decomposed into a constant parameter ℓ_θ and a disturbance term Δ_θ. For the constant part ℓ_θ, a conventional adaptive controller is designed, which uses $\hat{\theta}$ to estimate ℓ_θ. For the disturbance term Δ_θ, a combination of high-gain robust control and sliding mode control is utilized to compensate for its effects. The same approach is applied to the time-varying parameter $b(t)$. Since the final output of this controller is the derivative of the control output $\dot{u}$, an integration step is required to obtain the actual control output u. This design inherently avoids abrupt changes in the control output caused by the introduction of sliding mode control (while $\dot{u}$ may change abruptly, its integral u remains smooth).

2.3. Stability analysis

To derive the update rates for $\hat{\theta}$ and $\hat{\rho}$ using a Lyapunov function, it is generally necessary to introduce $\theta(t)$ and $b(t)$ into the function. However, this leads to the introduction of the derivatives of $\theta(t)$ and $b(t)$ during the differentiation of the Lyapunov function. Thanks to the introduction of the congelation of variables method, $\hat{\theta}$ and $\hat{\rho}$ are now the estimated values of ℓ_θ and $\frac{1}{\ell_b}$, respectively. Therefore, this issue can be resolved by simply replacing $\theta(t)$ and $b(t)$ with ℓ_θ and $\frac{1}{\ell_b}$. In the light of this, consider the modified Lyapunov function candidate:

$$V = \frac{1}{2} e^2 + \frac{1}{2\alpha} (\ell_\theta - \hat{\theta})^2 + \frac{|\ell_b|}{2\gamma} (\frac{1}{\ell_b} - \hat{\rho})^2 \tag{11}$$

Taking the derivative of this equation along the trajectories of Equation (6) yields:

$$\dot{V} = [\hat{\theta}f + \Delta_\theta f + (\ell_\theta - \hat{\theta})f + \Delta_b\hat{\rho}\bar{u} - \ell_b(\frac{1}{\ell_b} - \hat{\rho})\bar{u}]e + \bar{u}e - \dot{f}_d e - \frac{\dot{\hat{\theta}}}{\alpha}(\ell_\theta - \hat{\theta}) - \frac{|\ell_b|\dot{\hat{\rho}}}{\gamma}(\frac{1}{\ell_b} - \hat{\rho}) \quad (12)$$

Substituting Equations (9) and (10) into Equation (12) yields:

$$\dot{V} = \hat{\theta}fe + \Delta_\theta fe + \bar{u}e + \Delta_b\hat{\rho}\bar{u}e - \dot{f}_d e \quad (12)$$

It is evident that$\dot{V} = 0$when$e = 0$. Therefore, the following discussion focuses on the case when$e \neq 0$. First, to address the term$\Delta_b\hat{\rho}\bar{u}e$, Equation (8) can be rewritten as:

$$\bar{u} = -\xi(e,f) \cdot e \quad (13)$$

$$\xi(e,f) = k + \delta_\theta|f|\frac{1}{|e|} + \left|\dot{f}_d\right|\frac{1}{|e|} + \frac{1}{2}(\varepsilon_\theta + \frac{\hat{\theta}^2 f^2}{\varepsilon_\theta})\frac{1}{|e|} \quad (14)$$

Obviously, $sgn(e) = \frac{e}{|e|}$ when $e \neq 0$, hence $\xi(e,f) > 0$. Substituting Equation (14) into Equation (10) yields $\dot{\hat{\rho}} = \gamma\xi e^2 \cdot sgn(\ell_b)$. Since $b(t) > 0$ for all $t \geq 0$, and $0 < \ell_b < b(t)$, it follows that$\dot{\hat{\rho}} > 0$and$\Delta_b = b(t) - \ell_b > 0$. This implies that if the initial condition satisfies$\hat{\rho}(0) > 0$, then $\hat{\rho}(t) > 0$ holds for all$t \geq 0$. Consequently, $\Delta_b\hat{\rho}\bar{u}e = -\Delta_b\hat{\rho}\xi e^2 < 0$for all$t \geq 0$. Finally, substituting Equation (8) into Equation (13) gives:

$$\dot{V} = -ke^2 + [\hat{\theta}fe - \frac{1}{2}(\varepsilon_\theta + \frac{\hat{\theta}^2 f^2}{\varepsilon_\theta})|e|] + (\Delta_\theta fe - \delta_\theta|f||e|) + \Delta_b\hat{\rho}\bar{u}e - (\dot{f}_d e + \left|\dot{f}_d\right||e|) \quad (16)$$

In the stability analysis of classical adaptive control, the derivative of its Lyapunov function is $\dot{V} = -ke^2$. Using Barbalat's Lemma, the conclusion that the error e asymptotically converges to zero can be readily drawn. For Equation (16), it is evident that $\dot{V} \leq -ke^2 \leq 0$. Therefore, we can conclude that all trajectories of the closed-loop system are bounded and the error e asymptotically converges to zero.

3. Simulations

To objectively evaluate the performance of the proposed controller, simulations are conducted in which it is compared with a classical adaptive controller. The classical adaptive controller is presented below:

$$u = \hat{\theta}\dot{f}_d - ke \quad (15)$$

$$\dot{\hat{\theta}} = -\alpha\dot{f}_d e \quad (16)$$

where k and α are the force gain and adaptive gains, respectively. $\hat{\theta}$is the adaptive parameter.

Consider the following nonlinear system with time-varying parameters:

$$[2sin(2\pi t) + 12]f = v^{0.4} + 2 \quad (17)$$

$$f_d = 5 \quad (18)$$

The case of a constant desired force is first considered in the simulation. To ensure a fair comparison, the parameters for both controllers are set to the same values: $k = 1$, $\alpha = 1$, $\gamma = 1, \varepsilon_\theta = 10$. Based on the formulas $\theta(t) = \frac{-\hat{a}}{a}$, $\Delta_\theta = \theta(t) - \ell_\theta, \delta_\theta \geq max(|\Delta_\theta|)$, we select $\ell_\theta = 0$ and $\delta_\theta = 1.07 > max(|\Delta_\theta|) = 1.062$ for this system. While other values could be chosen, a larger δ_θ would increase the control output (in practice, selecting $\delta_\theta = 1.07$ corresponds to choosing $\ell_\theta = \pm 0.008$). The initial conditions for both controllers are set to $\hat{\theta}(0) = 0$, $u(0) = 0$. Since for all $t \geq 0$, $\hat{\rho}(t) > 0$, we choose to set the initial value of $\hat{\rho}(t)$ as $\hat{\rho}(0) = 0.01$.

The simulation results are shown in Figure 2. Controller 1 is the adaptive force controller proposed in this paper, while Controller 2 is the classical adaptive controller. It is evident that the tracking error of the closed-loop system with Controller 1 converges asymptotically, whereas the tracking error of the system with Controller 2 does not converge. For Controller 1, the time for the error to decrease from -5 to -0.5 is 0.483s, and the time for the parameter estimation $\hat{\theta}$ to rise from 0% to 90% of its final value is 0.438s. The overshoot of Controller 1 is 0.696%. Controller 2 has a rise time of 16.712 s and a maximum overshoot of 9.07%. Controller 1 exhibits not only very fast convergence of the tracking error but also rapid convergence of the parameter estimates $\hat{\theta}$. In the classical adaptive controller, since $\dot{\hat{\theta}} = -\alpha\dot{f}_d e$, $\dot{f}_d = 0$ and $\hat{\theta}(0) = 0$, it follows that for $t \geq 0$, $\hat{\theta}(t) = 0$, as shown in Figure 2(c).

To further validate the proposed controller's performance, the desired force is defined as a variable, described by:

$$f_d = sin(0.6\pi t) + 5 \quad (19)$$

The results obtained from the simulation are shown in Figure 3. The results of this simulation are consistent with the previous ones: the error e of the closed-loop system with Controller 1 converges asymptotically, whereas the system with Controller 2 does not converge. Controller 1 has a rise time of 0.432s, an overshoot of 1.058%, and the parameter $\hat{\theta}$ has a rise time of 0.391s. In contrast, Controller 2 has a rise time of 12.581s and an overshoot of 21.986%. The proposed adaptive force controller is capable of asymptotically and stably tracking the sinusoidally varying desired force, further demonstrating its feasibility, stability, and superior performance. Furthermore, in both simulations, $\hat{\rho} > 0$holds for all $t \geq 0$, which validates the correctness of the theoretical analysis presented earlier.

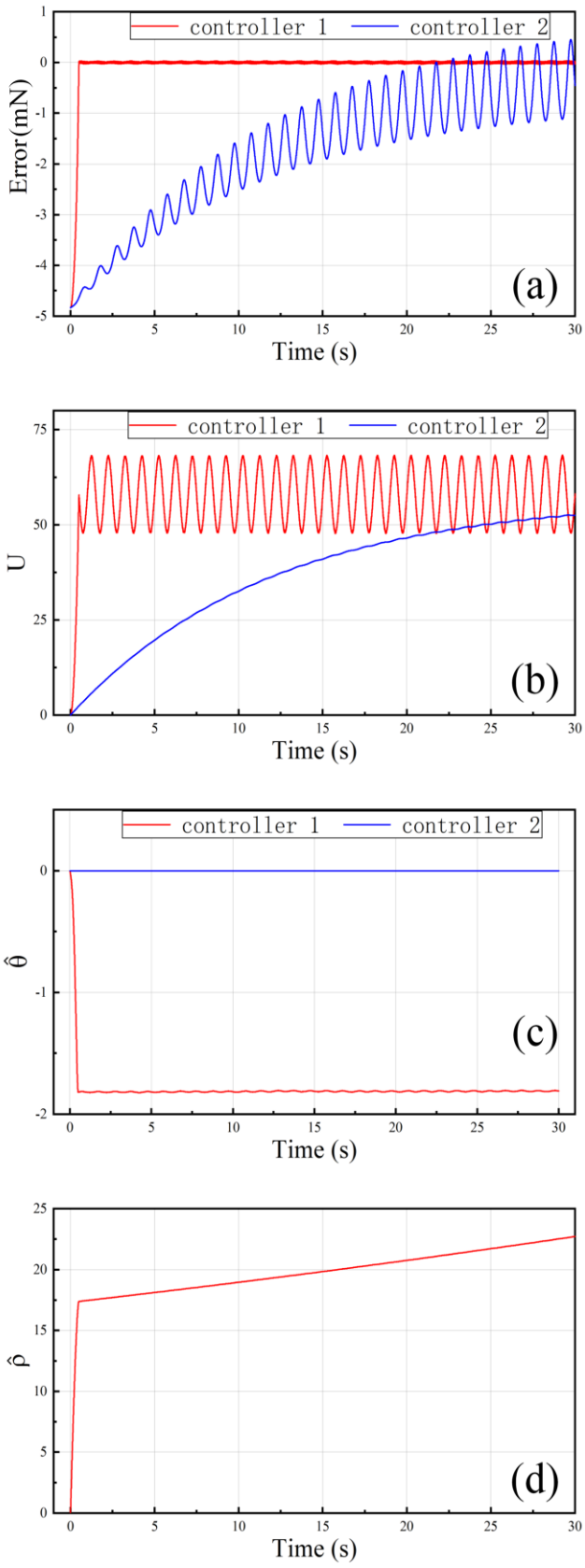

Fig. 2. (a) Tracking error, (b) control output, and (c),(d) parameter estimates versus time for the proposed controller and the classical adaptive controller during constant-force tracking simulation of a system with time-varying parameters.

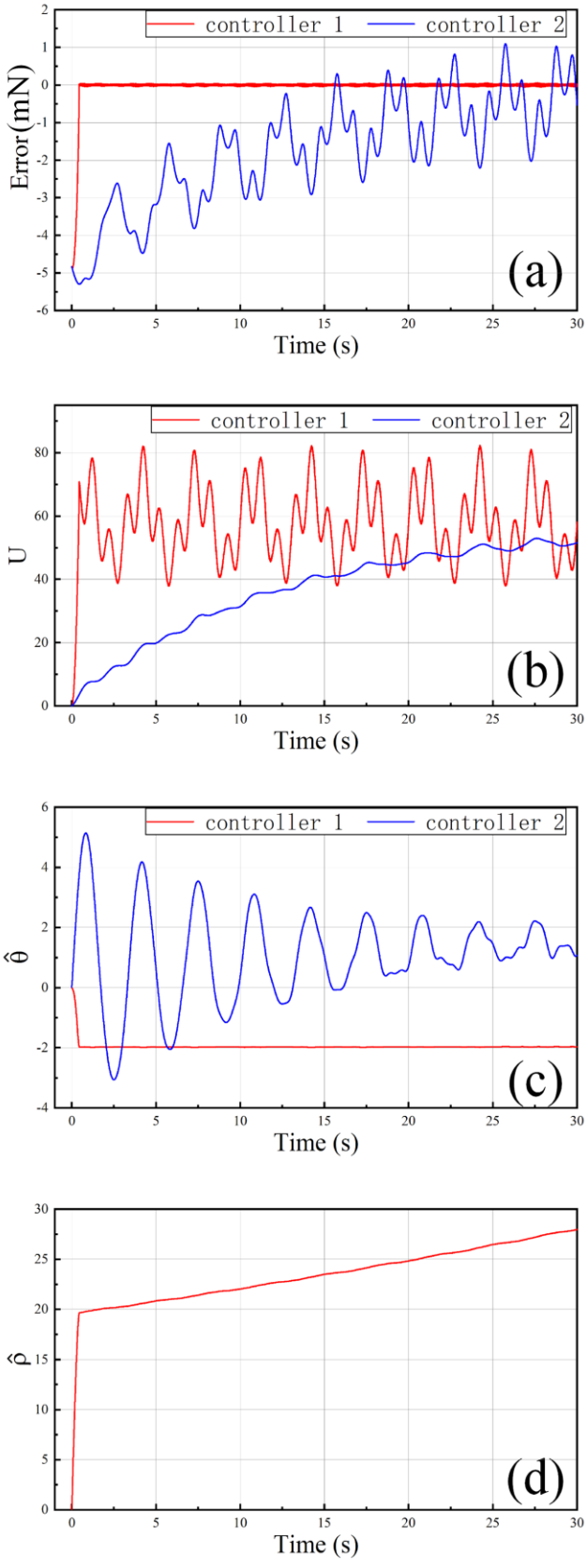

Fig. 3. (a) Tracking error, (b) control output, and (c),(d) parameter estimates versus time for the proposed controller and the classical adaptive controller during time-varying force tracking simulation of a system with time-varying parameters.

4. Experiments and result

The proposed controller was designed to achieve stable force control for the film peeling process. Therefore, robotic film peeling experiments were conducted to further validate its feasibility and performance.

4.1. Experimental setup

The robotic system used in this experiment consists of an ophthalmic microsurgery robot [22] and a robotic microsurgery forceps [23], as shown in Figure 4. The robotic microsurgery forceps are integrated with a 3D force sensor based on Fiber Bragg Grating (FBG) [24] and possess two degrees of freedom: rotation and grasping. The ophthalmic microsurgery robot has six degrees of freedom, with each joint controlled via a velocity loop. By mounting the robotic microsurgery forceps onto the end of the ophthalmic microsurgery robot, the experimental robotic system is established. To facilitate film adhesion, a stepped film mounting platform was fabricated using 3D printing. The primary functions of this platform are: 1) to position the film, ensuring a relatively consistent posture during each adhesion process, and 2) to provide a rigid substrate for film attachment. The film selected for peeling is a polyimide tape with a width of 1 mm and a thickness of 55μm. We used a depth-sensing camera to simultaneously measure the coordinates of both the film mounting platform and the robotic microsurgery forceps within the camera coordinate system (with the forceps already attached to the robot). Through coordinate transformation, the position of the film mounting platform relative to the robot's base coordinate system was obtained, providing essential data for subsequent kinematic planning.

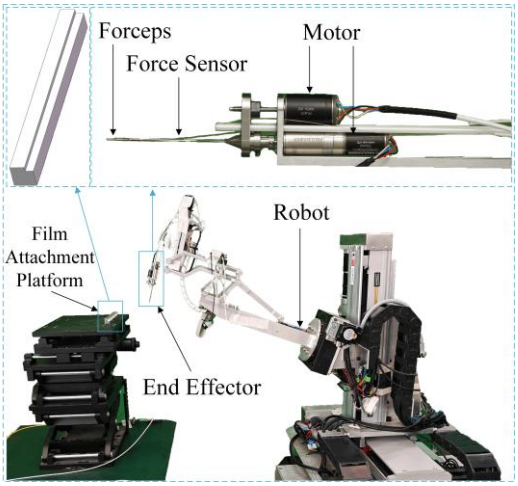

Fig. 4. Experimental setup.

An ideal schematic of the peeling process in the experiment is shown in Figure 5. According to the research by Peng et al., when only the peeling angle φ varies, the peeling force f is minimized at $\varphi = \frac{\pi}{2}$. Therefore, the objective of the kinematic design is to maintain $\varphi = \frac{\pi}{2}$ throughout the entire peeling process. Under this premise, it is evident that the distance the peeling front advances along the substrate equals the vertical lifting distance of the forceps, hence $v_{crack} = v_{peel}$. The end-effector velocity is $v_{end} = v_{crack} + v_{peel}$. Therefore, theoretically, the velocity of the end-effector should make an angle of $\frac{3\pi}{4}$ with the horizontal plane. The peeling force f, measured by the force sensor, is fed into the controller to compute v_{peel}. The required end-effector velocity v_{end} is subsequently determined through kinematics. Notwithstanding the kinematic planning, the actual peeling angle φ may deviate from the target value due to depth camera calibration errors and inaccuracies in manual film placement.

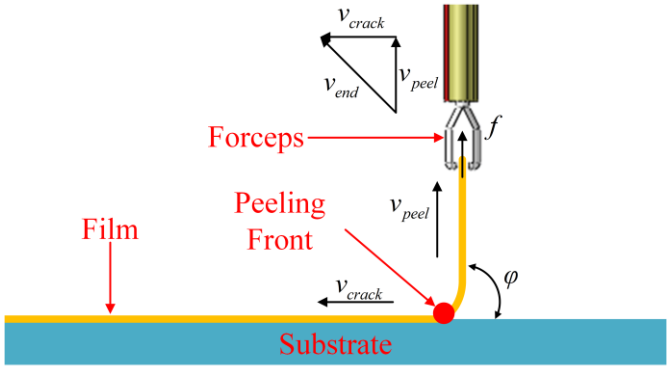

Fig. 5. Ideal schematic of the peeling process.

4.2. Preliminary experiment

According to the theory outlined in Section 2, the value of parameter δ_θ must be determined prior to conducting the experiment. Therefore, we first performed constant-speed tests to identify the variation range of parameter θ. Tests were conducted at three speeds: $v_{peel} = 1mm/s$, $v_{peel} = 2mm/s$, and $v_{peel} = 3mm/s$, with each speed repeated three times. To avoid excessive clutter in the figures, only one set of data for each speed is presented. The experimental results are shown in Figure 6.

As established in Section II, $a(t) \cdot f = v^n + m_0$ and $\theta(t) = \frac{-\dot{a}}{a}$. However, the experiment only provides the relationship between the peeling force and time. Therefore, methods are needed to determine the variation range of parameter θ. In the aforementioned experiments, the peeling speed was held

constant, allowing us to treat the term $v^n + m_0$ as an unknown constant. Consequently, the original dynamic equation can be rewritten as $f = \frac{n}{a}$, yielding the calculation formula for the parameter θ:

$$\frac{\dot{f}}{f} = \frac{-\dot{a}}{a} = \theta \tag{20}$$

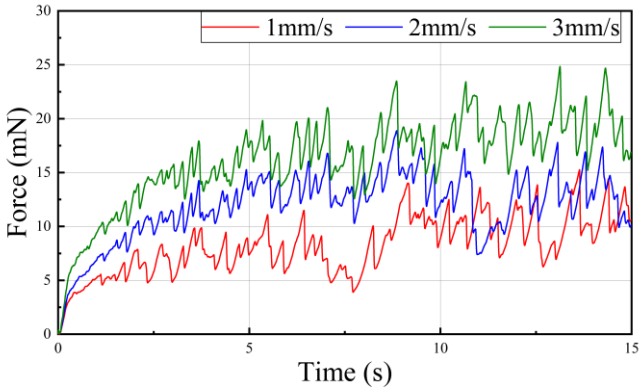

Fig. 6. A plot of peeling force versus time for a constant peeling speed.

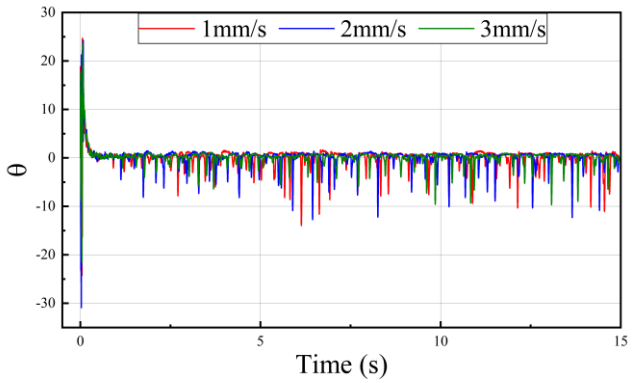

Fig. 7. A plot of parameter θ versus time for a constant peeling speed.

The relationship between parameter θ and time, obtained by substituting the results of the preliminary experiment into Equation (22), is shown in Figure 7.

The value of θ is significantly higher and changes more rapidly at the beginning of each experiment than during the stable phase, due to the initial non-steady-state peeling condition. This is corroborated by the corresponding transient rise in peeling force from zero at the onset of peeling, as shown in Figure 5 and consistent with findings in the Zhou et al. paper. Figure 6 clearly shows a decreasing trend in parameter θ during the initial experimental phase, which further confirms the non-steady-state peeling condition during this period. Additionally, the peeling force is very small at this stage. According to Equation (22), the excessively small denominator would significantly amplify the measurement error from the force sensor. For these two reasons, we consider the values of parameter θ during the first 500ms of the experiment unreliable and should be disregarded. Based on experimental results, the variation range of parameter θ was determined to be $[-14.66, 1.86]$. Therefore, we selected $\ell_\theta = -6.4$ and $\delta_\theta = 8.3 > max(|\Delta_\theta|) = 8.26$.

4.2. Result

Constant force tracking experiments were conducted by applying the result of $\delta_\theta = 8.3$ to our proposed controller, with the force setpoint set to $f_d = 15mN$. A total of six experiments were performed. Table 1 presents the statistical data from all five experiments, while the results of three representative experiments are shown in Figure 8.

Table 1. Summary of The Results of The Five Experiments.

Times	1	2	3	4	5
Max error(mN)	-1.452	-1.523	1.611	1.236	-1.561
RMSE(mN)	0.612	0.654	0.502	0.574	0.642
Mean error(mN)	-0.365	-0.487	0.354	-0.311	0.525

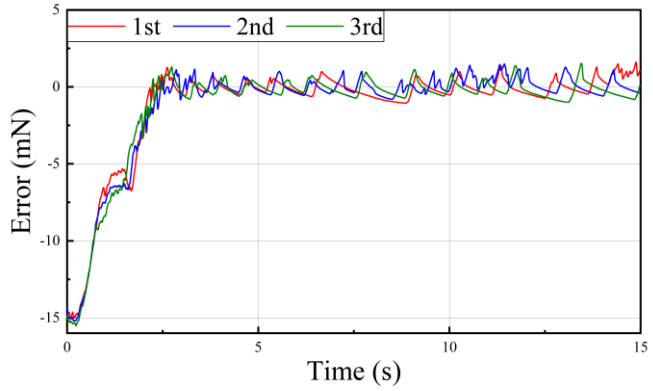

Fig. 8. Tracking error versus time for the proposed controller during force tracking Experiments.

Across the six experiments, the maximum error was 1.611mN, the maximum root mean square error (RMSE) was 0.642mN, and the maximum mean error was 0.525mN. (The statistics were calculated using data recorded after the error first reached 0mN.). Although the control output exhibited some oscillation, it remained within the tolerable range for the robotic arm. The results demonstrate that the proposed control method can effectively enable the robotic arm to track the desired peeling force.

We believe the discrepancies between the experimental and simulation results are primarily attributable to differences between the theoretical and the actual dynamic models of the film peeling process. We attribute these modeling errors to two main factors: 1) errors introduced by the deformation of the adhesive tape itself, and 2) errors arising from the deformation

of the forceps.

The experiments were conducted using an ophthalmic surgical robotic system. The force sensor integrated into this system has a range of $[0mN, 25mN]$, necessitating that the peeling force be constrained within this limited range. This requirement, in turn, compelled the use of an adhesive tape with a smaller width. Consequently, the polyimide tape employed in this experiment has a width of only 1 mm. Despite the grooves on the rigid platform designed to assist film alignment, manual placement cannot guarantee perfect parallelism between the film and the platform's axis. Consequently, the film inevitably undergoes varying degrees of twisting during the peeling process. Given the small width-to-thickness ratio of the tape, the forces induced by its own twisting and deformation cannot be neglected, leading to a deviation between the actual physical process and the theoretical model.

During the experiments, we observed occasional deformation of the forceps when the end-effector velocity was high. When deformation occurs, the actual end-effector velocity of the robotic system is lower than the desired velocity. This indicates that forceps deformation introduces velocity hysteresis. This phenomenon suggests that when the controller's output is high, the robotic system's end-effector velocity cannot accurately track the desired velocity, meaning the input to the peeling system does not equal the controller's output. The combination of these two issues results in a large force-tracking error and prevents its convergence.

5. Conclusion

This paper formulates a force control problem for a nonlinear model with time-varying parameters, motivated by the practical task of robotic film peeling. To address this problem, a force controller based on the congelation of variables and sliding mode control theory is proposed. The controller ensures asymptotic convergence of the force tracking error, as proven via a Lyapunov function. Furthermore, an integral action is incorporated to eliminate abrupt changes in the control output caused by the introduction of sliding mode control. Simulation results demonstrate the asymptotic tracking capability of the proposed controller, and a comparative study with a traditional adaptive controller highlights its superior performance. Finally, experimental results validate the feasibility and stability of the proposed approach.

References

1. Nakata K, Ohji M, Ikuno Y, Kusaka S, Gomi F, Tano Y. Sub-retinal hemorrhage during internal limiting membrane peeling for a macular hole. Graefe's Arch Clin Exp Ophthalmol 2003; 241: 582–584. https://doi.org/10.1007/s00417-003-0676-y.
2. Peng Z, Wang C, Chen L, Chen S. Peeling behavior of a viscoelastic thin-film on a rigid substrate. International Journal of Solids and Structures 2014; 51(25–26): 4596–4603. https://doi.org/10.1016/j.ijsolstr.2014.10.011.
3. Yin H, Ma Y, Feng X. Rate-dependent peeling behavior of the viscoelastic film-substrate system. International Journal of Solids and Structures 2024; 286: 112588. https://doi.org/10.1016/j.ijsolstr.2023.112588.
4. Yin H, Wang Z, Jiao Y, Zhang Y, Ma Y, Feng X. Interfacial competing fracture in peeling of bi-interface film-substrate system. Journal of the Mechanics and Physics of Solids 2025; 203: 106216. https://doi.org/10.1016/j.jmps.2025.106216.
5. Narendra K, Annaswamy A. Stable adaptive systems. Englewood Cliffs, NJ, USA, Prentice Hall: 1989.
6. Krstic M, Kokotovic P, Kanellakopoulos I. Nonlinear and adaptive control design 1st ed. New York, NY, USA, Wiley: 1995.
7. Ioannou P, Sun J. Robust adaptive control. Upper Saddle River, NJ, Prentice-Hall: 1996.
8. Tao G. Adaptive control design and analysis. Hoboken, NJ, USA, Wiley: 2003.
9. Astolfi A, Karagiannis D, Ortega R. Nonlinear and adaptive control with applications. London, UK, Springer: 2007.
10. Song T, Fang L, Qian Y. A novel robust adaptive impedance control scheme for contact force tracking with unknown environment. IEEE Robotics and Automation Letters 2025; 10(7): 6744–6751. https://doi.org/10.1109/LRA.2025.3568570.
11. Huang J, Tateo D, Liu P, Peters J. Adaptive control based friction estimation for tracking control of robot manipulators. IEEE Robotics and Automation Letters 2025; 10(3): 2454–2461. https://doi.org/10.1109/LRA.2025.3530159.
12. Kreisselmeier G. Adaptive control of a class of slowly time-varying plants. Systems and Control Letters 1986; 8(2): 97–103. https://doi.org/10.1016/0167-6911(86)90067-8.
13. Middleton R, Goodwin G. Adaptive control of time-varying linear systems, IEEE Transactions on Automatic Control 1988; 33(2): 150–

155. https://doi.org/10.1109/9.382.
14. Tsakalis K, Ioannou P. Adaptive control of linear time-varying plants. Automatica 1987; 23(4): 459–468. https://doi.org/10.1016/0005-1098(87)90075-6.
15. Zhang Z, Xie X, Ge S. Adaptive tracking for uncertain MIMO nonlinear systems with time-varying parameters and bounded disturbance. IEEE Transactions on Systems, Man, and Cybernetics: Systems 2021; 51(7): 4479–4491. https://doi.org/10.1109/TSMC.2019.2939042.
16. Marino R, Tomei P. Robust adaptive regulation of linear time-varying systems. IEEE Transactions on Automatic Control 2000; 45(7): 1301–1311. https://doi.org/10.1109/9.867023.
17. Marino R, Tomei P. Adaptive control of linear time-varying systems. Automatica 2003; 39(4): 651–659,. https://doi.org/10.1016/S0005-1098(02)00287-X.
18. Xu J. A new periodic adaptive control approach for time-varying parameters with known periodicity. IEEE Transactions on Automatic Control 2004; 49(4): 579–583. https://doi.org/10.1109/TAC.2004.825612.
19. Zhang Y, Ioannou P. Adaptive control of linear time varying systems. Proceedings of 35th IEEE Conference on Decision and Control 1996; 1: 837–842. https://doi.org/10.1109/CDC.1996.574516.
20. Zhang Y, Fidan B, Ioannou P. Backstepping control of linear time-varying systems with known and unknown parameters. IEEE Transactions on Automatic Control 2003; 48(11): 1908–1925. https://doi.org/10.1109/TAC.2003.819074.
21. Chen K, Astolfi A. Adaptive control for systems with time-varying parameters. IEEE Transactions on Automatic Control 2020; 66(5): 1986–2001. https://doi.org/10.1109/TAC..3046141.
22. Bai M, Zhang M, Zhang H, Pang L, Zhao J, Gao C. An error compensation method for surgical robot based on RCM mechanism. IEEE Access 2021; 9: 140747–140758. https://doi.org/10.1109/ACCESS.2021.3117350.
23. Zhang H, Yi H, Wang C, Yang J, Jin T, Zhao J. A robotic microforceps for retinal microsurgery with adaptive clamping method. IEEE/ASME Transactions on Mechatronics 2024; 29(6): 4492–4503. https://doi.org/10.1109/TMECH.2024.3378275.
24. Zhang H, Yi H, Fan Z, Pang L, Bai M, Wang C, Zhao J. An FBG-based 3-DOF force sensor with simplified structure for retinal microsurgery. IEEE Sensors Journal 2022; 22(15): 14911–14920. https://doi.org/10.1109/JSEN.2022.3187771.